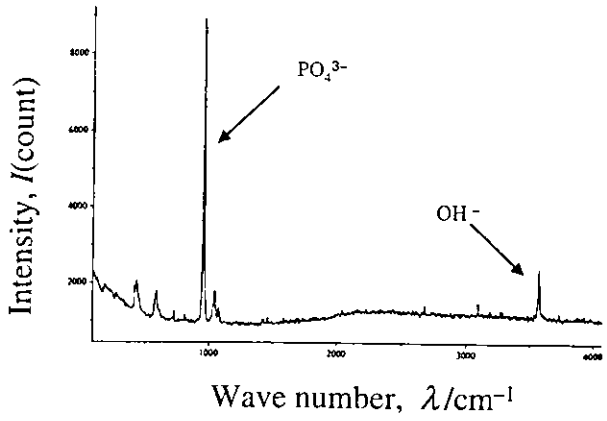

Fig. 5 Raman spectrum from 100%HAP region.

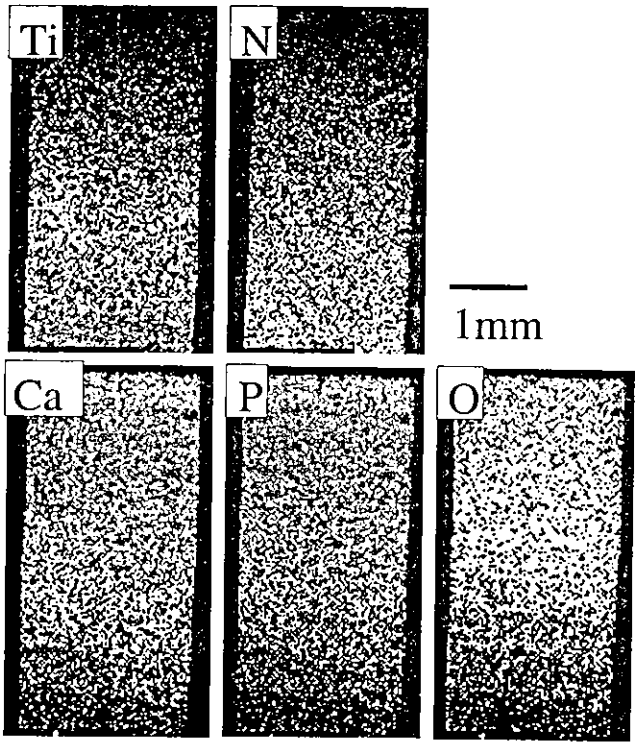

Fig. 6 EPMA elemental mapping of TiN/HAP FGM.

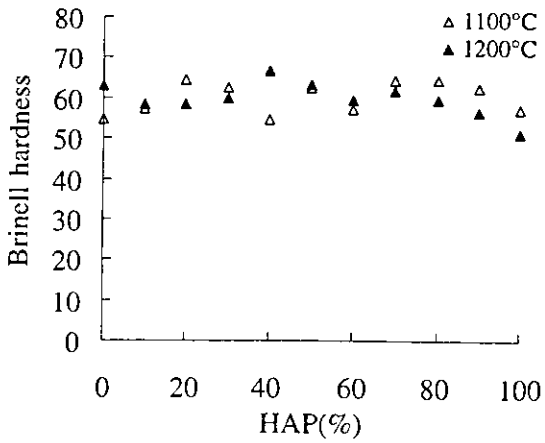

Fig. 7 Brinell hardness in each part of TiN/HAP FGM.

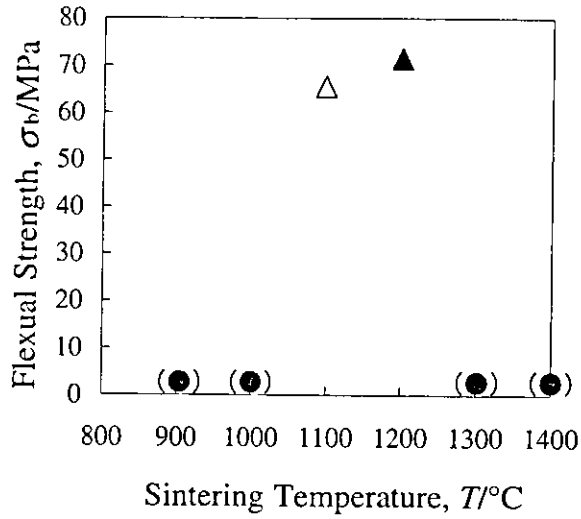

Fig. 8 Flexural strength of TiN/HAP FGM. (●): shows the auto-destructed specimens.

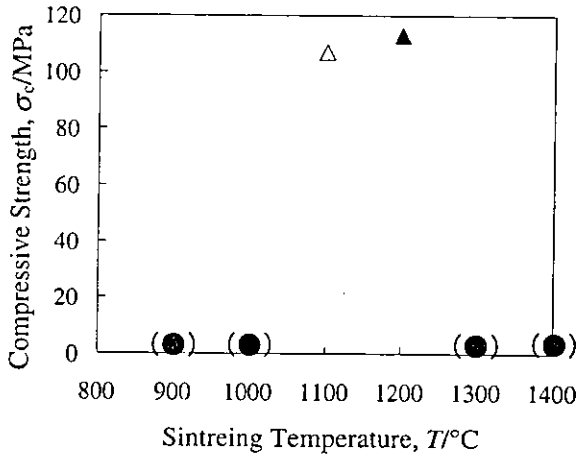

Fig. 9 Compression strength of TiN/HAP FGM. (●): shows the auto-destructed specimens.

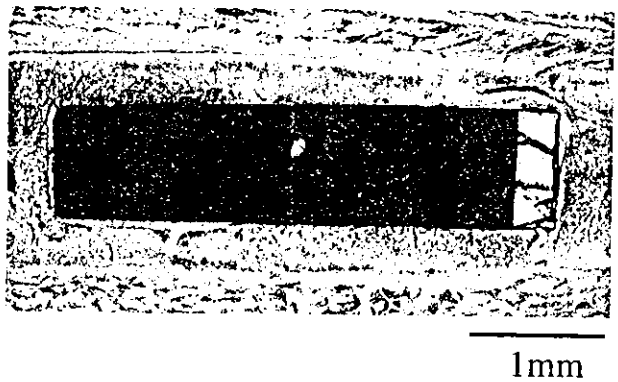

Fig. 10 Optical microscopic view of TiN/HAP FGM implant in diaphysis of femur after 8 weeks. (left: TiN, right: HAP).

HAP FGM after 2 week implantation, and the lower figures (c, d) show those after 8 weeks. In 2 weeks, an immature newly formed bone was observed around the TiN/HAP FGM. In 8 weeks, the newly formed bone around the

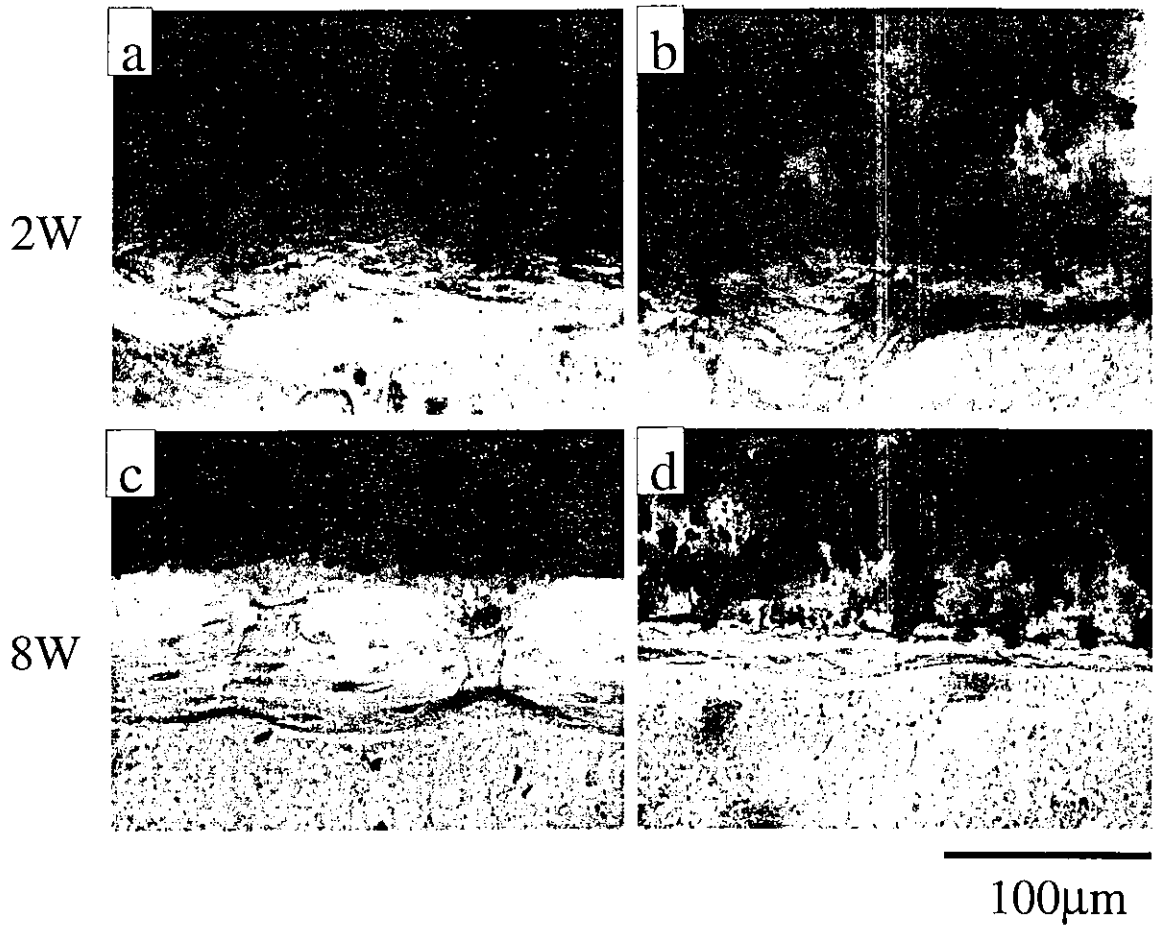

Fig. 11 Optical microscopic views of newly formed bone around TiN/HAP, after 2 weeks (a: HAP10 b: HAP90) and 8 weeks (c: HAP10 d: HAP90).

specimen was more matured. The thin lamilar structure was observed in a newly bone around the HAP rich region due to the bone remodeling (d), which was not observed at the Ti rich region (c). Very little inflammation was observed throughout the implantation period of 2 and 8 weeks.

Figure 12 shows the EPMA elemental mapping (Ca and Ti) of newly formed bone around TiN/HAP FGM after 8 week implantation. Inside the implant, Ca and Ti showed the gradient composition, complementary each other. The mapping of Ca, bone composition element, represents the formation of new bone around TiN/HAP FGM.

4. Discussion

4.1 Effect of SPS

The implant of simple substance, for example, HAP shows the high bone conduction.[1-3] However, there is a danger of fracture due to its brittle properties as dental implant when occlusal force is imposed. Ti implant has enough reliable mechanical properties. However, it takes more time until the formation of new bone after implantation, since bone conduction is inferior to HAP. In FGM which satisfies both bone conductivity and mechanical properties, it would be possible to lead a new bone to contact directly to implant material and to maturate from an early stage in root. In this study, TiN/HAP FGM was successfully fabricated by SPS.

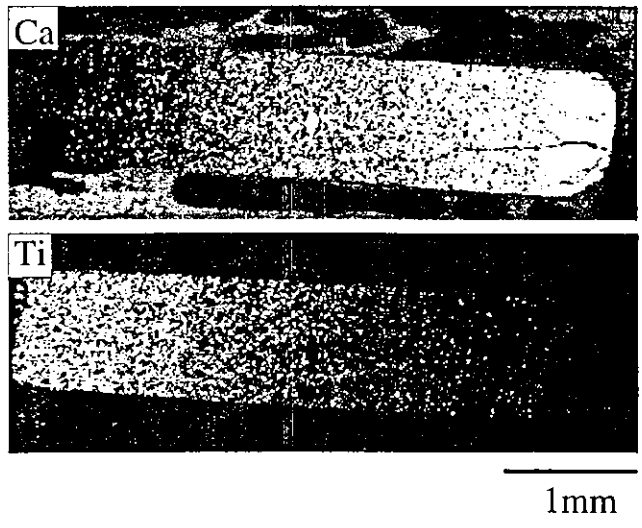

Fig. 12 EPMA elemental mapping of new bone formation around TiN/HAP inserted in diaphysis of femur for 2 weeks.

FGM is produced by intermingling two or more kinds of metals, ceramics or polymers. The optimal sintering conditions are usually different for these components and the formation of simultaneous sintering is difficult. SPS can promote the efficient and uniform sintering by generating

spark plasma between particles. This differs greatly from the conventional sintering using an electric furnace. Fabrication of stable Ti/HAP system FGM was limited up to Ti/Ti30%HAP, since heating at 1300°C was necessary to make sintering by electric furnace heating and FGM for lager content of HAP such as Ti/100%HAP was not possible.[13] By use of SPS, heating temperature could be lowered due to the enhancement of sintering and it was possible to fabricate Ti/100%HAP.[13–16] When pure Ti was used for FGM by SPS, 750°C was inadequate for sintering of Ti/HAP, but the self-destruction occurred after sintering at 900°C and 1000°C due to the decomposition of HAP.[15] The compromising optimum sintering temperature was found as 850°C.[15] When TiN was used for TiN/HAP FGM, the temperature of 900 and 1000°C was insufficient to endure to the mechanical shock at cutting. At 1300 and 1400°C, the self-destruction of specimens occurred after sintering, which was considered due to the decomposition of HAP. The sintering temperature was thus set as 1100 and 1200°C.

4.2 Mechanical properties of FGM

Since the composition and structure are changed from part to part in FGM, evaluation of their properties is not simple, compared with the homogeneous material. The Brinell hardness test evaluates the hardness in each part of FGM. Compression and flexural tests evaluate the representive value of mechanical strength for the whole sample. Brinell hardness test is suitable to evaluate a complex with porosity which can be measured from the depth of indentation using a spherical steel ball as indented. The hardness of TiN was very high (Hv~1300) nearly ten times of Ti.[19,20] In TiN region, sintering was inadequate and porous structure was observed by SEM (Figs. 3, 4). This resulted in the uniform Brinell hardness for the whole range in spite of the gradient composition from TiN to HAP.

The specimens sintered at 1100 and 1200°C had the flexural and compression strength of the similar level as a bone. Both strengths are slightly more improved for 1200°C than 1100°C, although the hardness of each part is nearly the same for the FGM sintered at 1100 and 1200°C. The results of compression and flexural tests for FGM are very much affected by existence of weak part. Since the mechanical properties of FGM are not uniform, fracture tends to initiate from crack formation at the weakest part, usually in the part of high ceramic content where sintering is insufficient, porosity is high and brittleness is predominant. Therefore the results of compression and flexural tests are not necessarily consistent with the Brinell hardness test. The most influential part for strength for the whole specimen is the degree of insufficient sintering in the TiN rich part, since 1100~1200°C is still insufficient for sintering of TiN whose melting point is 2950°C. The sintering at 1200°C improved the strength of TiN part, which thus resulted in the increase of compression and flexural strength compared with that of 1100°C.

4.3 Bone conductivity

Ti and HAP are widely used in clinics, because of high biocompatibility and bone conductivity. The chemically stable properties of TiN, especially the excellent corrosion resistance which may be better than Ti, would contribute to its biocompatibility.[17–20] Our previous study of implantation tests in the soft and hard tissue showed that TiN has the nearly equivalent biocompatibility as Ti and is suitable for the abrasion resistant implant which may be used for the abutment part of dental implant and the sliding part of artificial joint.[19,20]

In this study, the implantation experiment was conducted to observe the difference of the bone formation capability in each part of FGM. The rat femur was used for the implantation test since it is the largest space in rat for hard tissue which can hold a long specimen to compare the reaction for the composition from TiN to HAP in the longitudinal direction under nearly the same conditions. No inflammation was histopathologically observed on the surrounding of FGM in two and eight weeks after the direction and suture for implantation. EPMA elemental mapping was also performed for the analysis of hard tissue, where new bone formation was clearly recognized for the whole part around implant in Ca mapping. Theses confirmed that any part of TiN/HAP has biocompatibility. The further detailed observation by optical microscopy showed that the maturation of new bone was more advanced in the HAP rich region than in the Ti rich region. This suggests that a vital reaction in hard tissue changes in inclination in accordance to the inclination structure of material.

5. Conclusions

(1) By use of TiN instead of Ti, the decomposition of HAP could be suppressed.
(2) TiN/HAP FGM could be successfully fabricated at 1100 and 1200°C by SPS.
(3) The Brinell hardness was around 60, nearly uniform for the whole range of composition.
(4) Flexural strength of TiN/HAP FGM sintered at 1100°C and 1200°C showed 65.4 MPa and 71.3 MPa respectively, and compression strength of TiN/HAP FGM showed more than 100 MPa.
(5) The new bone was formed directly on the implants. No inflammation was observed throughout the implantation period of 2–8 weeks.
(6) In 8 weeks, the maturation of newly formed bone was more advanced in the HAP rich region.
(7) The sintering of TiN rich part was still insufficient for the temperature up to 1200°C.

Acknowledgements

Research was performed under Grant-in-Aid for Scientific Research (B) (2) from the Ministry of Education, Science, Sports and Culture of Japan, and Health and Laybour Sciences Research Grants in Research on Advanced Medical Technology from the Ministry of Health, Laybour and Welfare of Japan. The authors are grateful to Dr. Koichi OMAMYUDA of SUMITOMO OSAKA CEMENT for the supply of HAP.

REFERENCES

1) F. C. M. Driessens and R. M. H. Verbeeck: *Biominerals*, (CRC Press, Boca Raton, 1990) pp. 1.
2) H. Aoki: *Science and medical application of hydroxyapatite*, (Inc. Ishiyaku, Euro. America. Tokyo, 1994) pp. 1.
3) H. Aoki: *Medical applications of hydroxyapatite*, (Jap. Asso. Apatite. Science. Tokyo, 1991) pp. 1.
4) T. Hirai: *Materials Science and Technology. Processing of Ceramics Part 2*, vol. 17B, ed. by R. W. Cahn, P. Haasen and E. J. Kramer, (Weinheim, Verlagsgesellschaft, 1996) pp. 293–341.
5) F. Watari, A. Yokoyama, F. Saso, M. Uo and T. Kawasaki: *Functionally Graded Materials 1996*, ed. by I. Shiota Y. Miyamoto, (Elsevier, Amsterdam, 1997) pp. 749–754.
6) F. Watari, A. Yokoyama, F. Saso, M. Uo and T. Kawasaki: Composites Part B **28B** (1997) 5–11.
7) F. Watari, A. Yokoyama, F. Saso, M. Uo, H. Matsuno and T. Kawasaki: J. Japan Inst. Metals **62** (1998) 1095–1101. (in Japanese).
8) F. Watari, A. Yokoyama, F. Saso, M. Uo, H. Matsuno and T. Kawasaki: *Functionally Graded Materials 1998*, ed. by W. A. Kayser, (Trans Tech Publications, Zurich, 1999) pp. 356–361.
9) H. Takahashi, F. Watari, F. Nishimura and H. Nakamura: Dent. Mater. J. **11** (1992) 462–468.
10) F. Watari, A. Yokoyama, H. Matsuno, R. Miyao, M. Uo, Y. Tamura, T. Kawasaki, M. Omori and T. Hirai: *Functionally Graded Materials 2000, Ceramic Transaction 114*, ed. by K. Trumble, K. Bowman, I. Reimanis, S. Sampath, (Am. Ceramic Soc., 2001) pp. 73–80.
11) F. Watari, A. Yokoyama, H. Matsuno, R. Miyao, M. Uo, T. Kawasaki, M. Omori and T. Hirai: *Functionally Graded Materials in the 21st Century*, ed. by K. Ichikawa, (A Workshop on Trends and Forecasts, Kluwer Academic Publishers, Boston, 2001) pp. 187–190.
12) H. Takahashi: Dent. Mater. J. **12** (1993) 595–612.
13) F. Watari, A. Yokoyama, F. Saso, M. Uo and T. Kawasaki: *Proc. 3rd Int. Symp. Structural & Functionally Gradient Materials*, ed. by B. Ilschner, N. Cherradi, (Polytechniques Press, Romandes, Lausanne, 1995) pp. 703–708.
14) F. Watari, M. Omori, T. Hirai, A. Yokoyama, H. Matsuno, M. Uo, R. Miyao, Y. Tamura and T. Kawasaki: J. Jpn. Soc. Powder & Powder Metallurgy **47** (2000) 1226–1233.
15) R. Miyao, A. Yokoyama, F. Watari and T. Kawasaki: J. Jpn. Soc. Dent. Mater and Devices **20** (2001) 344–355. (in Japanese).
16) F. Watari, A. Yokoyama M. Omori, T. Hirai, H. Kondo, M. Uo and T. Kawasaki: Compos. Sci. Tech. **64** (2004) 893–908.
17) H. Matsuno, A. Yokoyama, F. Watari, M. Uo and T. Kawasaki: J. Jpn. Soc. Dent. Mater and Devices **8** (1999) 447–462. (in Japanese).
18) H. Matsuno, A. Yokoyama, F. Watari, M. Uo and T. Kawasaki: Biomaterials **22** (2001) 1253–1262.
19) Y. Tamura, A. Yokoyama, F. Watari and T. Kawasaki: Dent. Mater. J. **21** (2002) 355–372.
20) Y. Tamura, A. Yokoyama, F. Watari, M. Uo and T. Kawasaki: Mater. Trans. **43** (2002) 3043–3051.

NANO LETTERS

2005
Vol. 5, No. 1
157−161

Biological Behavior of Hat-Stacked Carbon Nanofibers in the Subcutaneous Tissue in Rats

Atsuro Yokoyama,*,† Yoshinori Sato,‡ Yoshinobu Nodasaka,† Satoru Yamamoto,† Takao Kawasaki,† Masanobu Shindoh,† Takao Kohgo,† Tsukasa Akasaka,† Motohiro Uo,† Fumio Watari,† and Kazuyuki Tohji‡

Graduate School of Dental Medicine, Hokkaido University, and Graduate School of Environmental Studies, Tohoku University

Received September 17, 2004; Revised Manuscript Received November 6, 2004

ABSTRACT

The tissue response to hat-stacked carbon nanofibers (H-CNFs) was evaluated. H-CNFs were implanted in the subcutaneous tissue of rats. Histological and ultrastructural investigations were carried out by transmission electron microscopy. Although many macrophages and foreign body giant cells were seen around H-CNFs, no severe inflammatory response such as necrosis was observed. Some H-CNFs were observed in lysosomal vacuoles of phagocytes. These results showed that H-CNFs were not strong prophlogistic substances and were englobed in vivo.

Medical applications of nanoscale substances such as carbon nanotubes (CNTs) and fullerenes have attracted a great deal of attention. In particular, nanoscale substances are indispensable for the development of new drug delivery systems and scaffolds. There have been some reports on the use of CNTs and fullerenes for biomaterials.[1−8] Most of them were studies in vitro such as on scaffolds for cell culture.[1−3, 5,6] Recently, toxicity of CNTs was reported, and their safety as biomaterials has been questioned.[9−20] Thus, the investigation of tissue responses, including in animal experiments in addition to in vitro studies, is necessary to evaluate toxicity and biocompatibility of nanoscale substances and to develop them for medical devices. However, there are only a few reports about tissue reactions to nanoscale substances.[11,12,19,20] We have studied nanocarbon materials as one of the nanoscale substances for biomaterials.[7,8,21,22] Sato et al. developed a colloidal dispersion of a new type of carbon nanofibers (CNFs) for application to biomaterials.[23] As their structure was similar to stacked hats, they named them hat-stacked carbon nanofibers (H-CNFs). H-CNFs with a novel graphene structure would be more suitable for biomaterials, because it is possible to control their size and to make them soluble in water. The purpose of this study was to investigate the tissue response in subcutaneous tissue and evaluate biocompatibility of H-CNFs for the first time.

H-CNFs were produced with a thermal CVD method using a powdered Ni catalyst in a conventional flow reactor system according to the report by Rodriguez.[24,25] The powdered Ni catalyst is placed in an Al_2O_3 boat positioned in a horizontal quartz tube furnace. The sample is initially reduced in a 10% hydrogen/helium stream for 120 min at 873 K. C_2H_4/H_2 (4:1) mixture gas is then introduced and reacted at 873 K for 4 h. Then, 100 mg of the produced soot is introduced into a flask with a reflux attachment together with 500 mL of 6 M hydrochloric acid for 12 h at 373 K. After HCl-reflux treatment, the suspension is filtered using a membrane filter with 0.1 μm apertures. Next, the filtered cake is transferred into a flask with 1.0 L of 6 M HNO_3 and refluxed at 373 K for 12 h to perfectly dissolve residual nickel. After the suspension is filtrated using a membrane filter of 0.1 μm apertures, the filtered cake is subsequently washed and finally dried for 24 h at 333 K. The measurement was carried out by scanning electron microscopy (SEM; S-4100, Hitachi, Japan) and transmission electron microscopy (TEM; HF-2000, Hitachi, Japan) in situ using energy-dispersive X-ray spectroscopy with ultrathin window, which is detectable for the atoms heavier than the atomic number 5 (B) (EDXS; Vantage EDX system, NORAN Instruments). The scheme, EDX analysis, SEM, and TEM of H-CNFs are shown in Figure 1. The structure of H-CNFs resembles bamboo hats stacked up toward a needle axis. Lengths of CNFs range approximately between 100 nm and 1 μm, and their diameters are between 30 and 100 nm, respectively. Ni was not detected by inductively coupled plasma optical emission spectrometry (ICP OES; Thermo elemental Co. Ltd., USA) and X-ray fluorescence analysis (XRF; MESA-500W, Horiba, Japan).

Eight male 6-week-old Wistar strain rats were used in this study. Under general anesthesia, incisions were made bilater-

* Corresponding author. Graduate School of Dental Medicine, Hokkaido University, Kita13, Nishi7,Kita-ku,Sapporo 060-8586, Japan. Tel: +81-11-706−4270. Fax: +81-11-706-4903. E-mail: yokoyama@den.hokudai.ac.jp
† Hokkaido University.
‡ Tohoku University.

10.1021/nl0484752 CCC: $30.25
Published on Web 12/08/2004

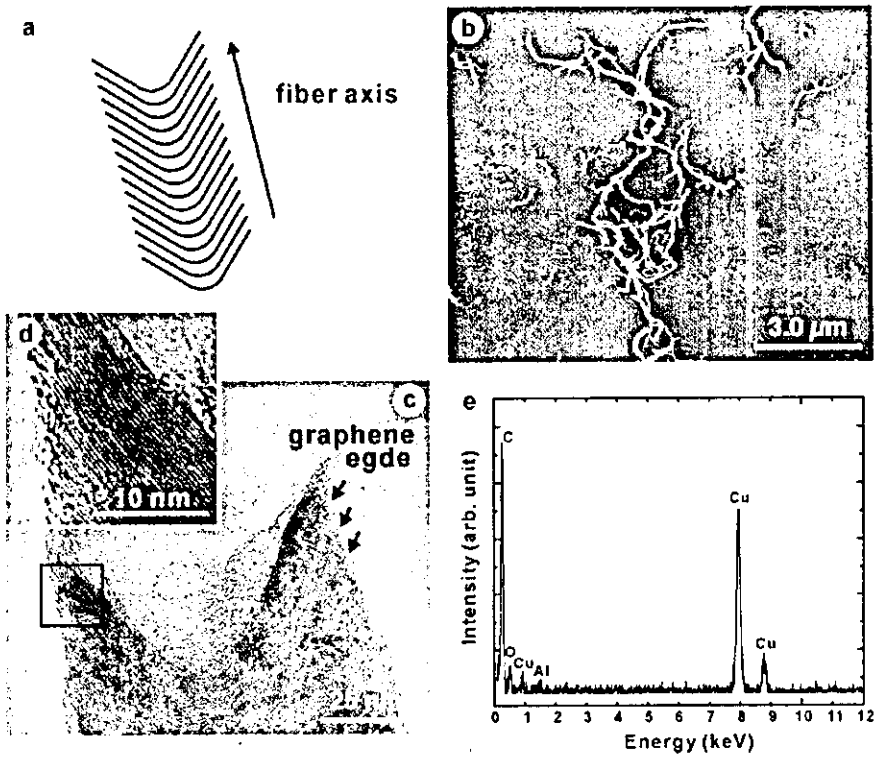

Figure 1. H-CNFs. (a) Scheme of H-CNFs. (b) SEM image of H-CNFs. (c) TEM image of CNFs. (d) High magnification of c. (e) EDX analysis of H-CNFs. The peaks of Cu and Al were due to the TEM grid made of cupper and the holder for the TEM grid, respectively.

ally in the thoracic region. Two pockets were made in the subcutaneous tissue. Clusters of H-CNFs were implanted in the subcutaneous tissue in the thoracic region bilaterally in each rat. Animal experiments were performed in accordance with the *Guide for the Care and Use of Laboratory Animals*, Hokkaido University Graduate School of Dental Medicine. During the course of the study, no rats were lost.

The rats were sacrificed at 1 and 4 weeks after surgery. Segments of the subcutaneous tissue including H-CNFs were excised and fixed. The fixed specimens were divided into two parts. One part was embedded in paraffin. Hematoxylin and eosin-stained specimens were observed by optical microscopy. The other was observed by TEM. The field observation by TEM was confirmed to be exactly consistent with that observed by optical microscopy. TEM specimens were postfixed with 1% OsO_4 and routinely embedded in epoxy resin after dehydration. Ultrathin sections (80 nm approximately) were cut with a diamond knife and stained with uranyl acetate and lead citrate. Stained sections were placed on a supporting carbon mesh grid and observed using a TEM operating at a voltage of 75 kV (H-800, Hitachi, Japan).

At 1 week after implantation, clusters of H-CNFs were surrounded by granulation tissue with a slight inflammatory change. Many mesenchymal cells, macrophages, and foreign body giant cells were observed around H-CNFs. The appearance was like foreign body granuloma (Figure 2a). High-magnification observation revealed that some H-CNFs were englobed by macrophages (Figure 2b). At 4 weeks, clusters of H-CNFs were surrounded by fibrous connective tissue (Figure 2c). Many foreign body giant cells were attached to H-CNFs (Figure 2d). No severe inflammatory response such as necrosis, degeneration, or neutrophil infiltration was observed around H-CNFs throughout the experimental period.

H-CNFs were observed in intercellular and intracellular spaces at 1 week after implantation (Figure 3a). Some of them were recognized in phagocytes with many vacuoles such as macrophages (Figure 3b). Lengths of H-CNFs were approximately between 100 nm and 1μm (Figure 3b). Many H-CNFs in phagocytes were aggregated (Figure 3c and d). Some H-CNFs in phagocytes were covered by a membrane (white arrows in Figure 3d), presumably a lysosomal membrane. There were no changes in the form of the H-CNFs after phagocytosis. The characteristic structures such as the stacked hats were still observed (Figure 3d).

At 4 weeks after implantation, H-CNFs were observed in phagocytes with a lot of vacuoles (Figure 4a). Although the characteristic form of H-CNFs, the hat-stacked shape, was recognized, the covering lysosomal membranes were seldom observed and the degree of aggregation was decreased (Figure 4b and c) in comparison with that at 1 week. Furthermore, H-CNFs looked shorter (Figure 4b) than those at 1 week and some H-CNFs appeared translucent (white arrow in Figure 4d), which was not observed at 1 week (Figure 4c and d).

Although it is desirable for carriers such as DDS and genes transfection to be water soluble, it is difficult to make CNTs soluble in water due to their chemical properties and shape with the μm length. H-CNFs have the characteristic structure that the edges of the stacked graphene layers are exposed at the surface. Therefore, many hydrophilic groups can be added

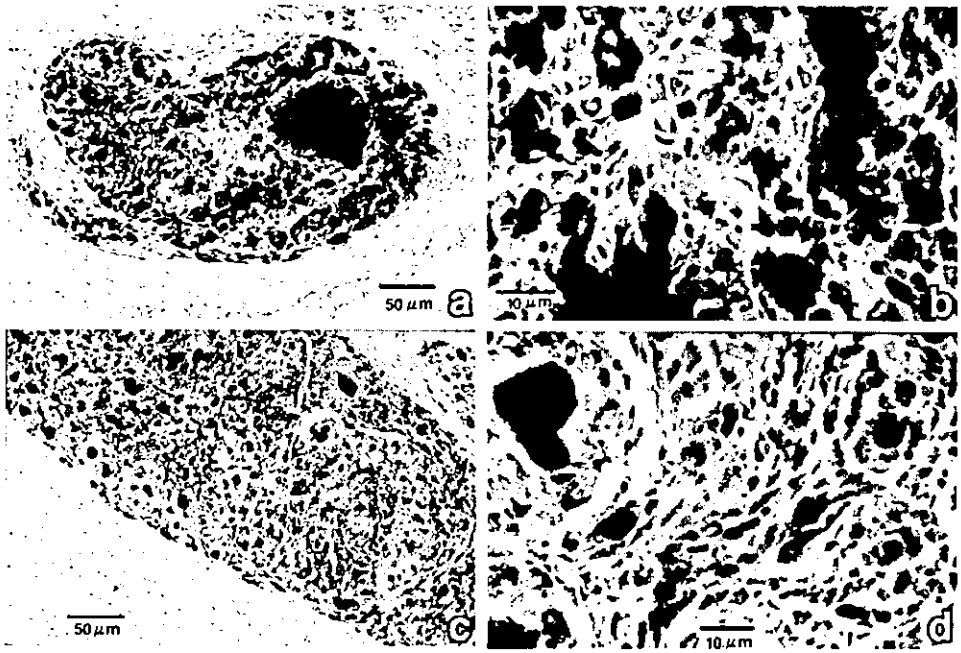

Figure 2. Histology of CNFs implanted in the subcutaneous tissue. (a) At 1 week. Clusters of CNFs were covered by granulation tissue. H. E. stain. (b) High magnification of a. Numerous macrophages and mesenchymal cells were observed around CNFs. (c) At 4 weeks. Clusters of CNFs were surrounded by fibrous connective tissue. H. E. stain. (d) High magnification of c. There were many foreign body giant cells attached to CNFs. H. E. stain.

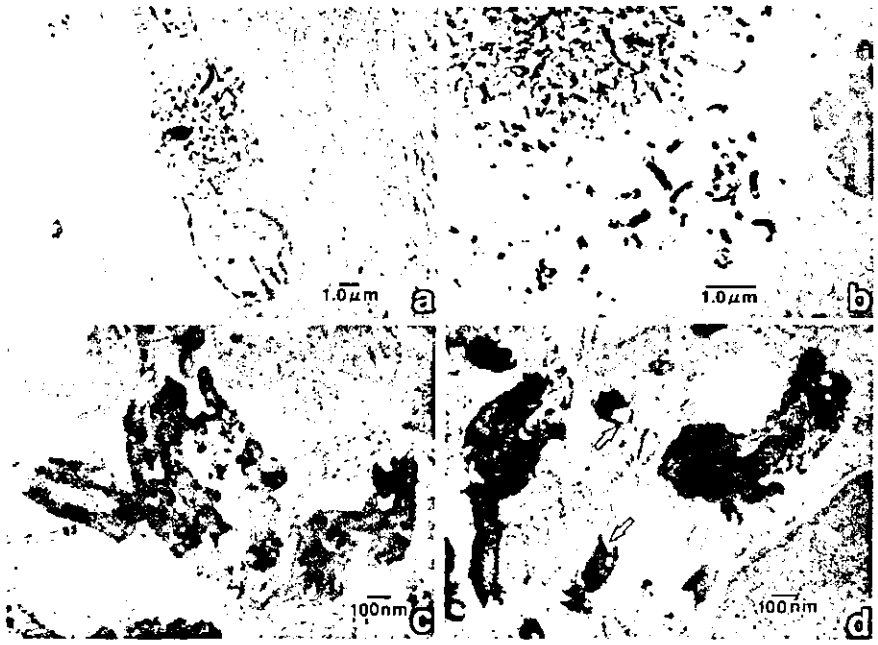

Figure 3. TEM images of CNFs implanted in the subcutaneous tissue at 1 week. (a) CNFs were observed in the cytoplasm of macrophage. (b) Various sizes of CNFs were observed in macrophage. (c) Many of CNFs in the phagocytes were aggregated. (d) Structure of membrane (white arrows) was observed around some of the CNFs.

and give water solubility to H-CNFs. Since the binding force between each graphene sheet originating from van der Waals force is rather weak, it is easy to cut and control the sizes of H-CNFs. Therefore, H-CNFs are suitable as a carrier of DDS and we investigated the tissue reaction of H-CNFs in this study.

The toxicity of nanoscale substances has been suggested recently.[9,20] Huczko et al. reported that CNTs containing soot synthesized from a catalyst-doped (Co/Ni) graphite anode by an arc discharge method did not induce any abnormalities of pulmonary function or measurable inflammation in guinea pigs, and that fullerene soot with a high

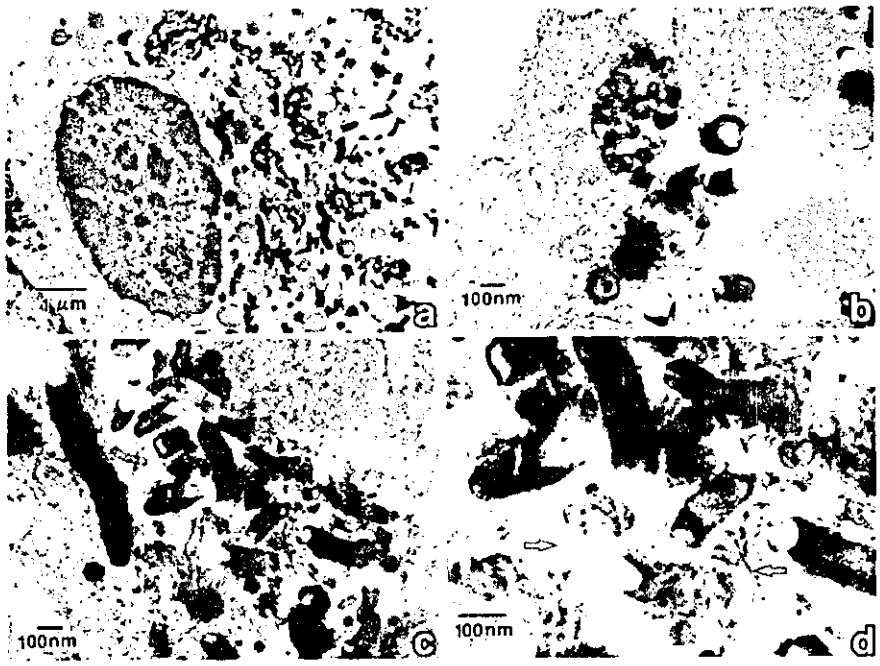

Figure 4. TEM images of CNFs implanted in the subcutaneous tissue at 4 weeks. (a) CNFs were observed in macrophage. (b) Smaller CNFs were observed compared with those at 1 week. (c) The degree of aggregation of CNFs was lower than that at 1 week. (d) Some CNFs (white arrows) became translucent.

content of single-walled carbon nanotubes (SWCNTs) did not induce any skin hazards.[11,12] On the other hand, Lam et al. investigated the pulmonary toxicity of SWCNTs using mice.[20] They reported that SWCNTs induced dose-dependent epithelioid granulomas and interstitial inflammation at 7 days, and peribronchial inflammation and necrosis at 90 days after intratracheal instillation, while carbon black as a control did not induce any severe inflammatory change. They considered that the difference of pulmonary toxicity between carbon nanotubes and carbon black was related to the physicochemical properties and fibrous structure of carbon nanotubes. Warheit et al. reported that SWCNTs instilled intratracheally induced granulomatous inflammation that was not dose dependent in rats, and that the cytotoxicity was perplexing.[21] In this study, although granulomatous inflammatory change around H-CNFs was observed at 1 week after implantation, they were surrounded by thin fibrous connective tissue at 4 weeks. These observations indicate that the organization process of inflammation for foreign bodies proceeded with time. Furthermore, no severe inflammatory response such as necrosis or invasion of neutrophils was observed. These results suggest that H-CNFs are not acutely toxic in the subcutaneous tissue. It seemed that wound healing was not inhibited, because slight inflammatory changes were observed only close to H-CNFs, while the control skin incisions were not done. These different results of our study from those of Lam et al. may be caused by the physicochemical properties of H-CNFs, for example, water solubility and the characteristic structure composed of the stacked graphene hats, apart from the implant site and species of the animals.

Observation by TEM revealed that H-CNFs implanted in the subcutaneous tissue were phagocytosed by macrophages. Foreign objects are englobed in macrophages in the inflammatory response. Titanium particles from dental and medical implants were recognized in macrophages by TEM observation in some reports.[26,27] Although cytostructures such as membranes of lysosomes were observed around most H-CNFs inside the phagocytes at 1 week, they were not observed at 4 weeks after implantation. The degree of aggregation of H-CNFs decreased from 1 week to 4 weeks. The H-CNFs appeared to become shorter with time, although quantification was not carried out. Furthermore, some of H-CNFs were translucent. These changes of structure in H-CNFs that occurred in lysosomes and cytoplasm might be related to the characteristics of H-CNFs. Delamination of layered materials by intercalation reactions has been reported.[28,29] In this study, delamination of graphene layers of H-CNFs could have originated from the intercalation of hydrophilic substances such as enzymes and proteins in lysosomes and cytoplasm related to rich functional groups resulting from exposure of the edges of the graphene hats. Decrease of fiber length of H-CNFs would occur subsequently. In addition, the energy of cytoplasmic motion[30] might be involved in the shortening of the H-CNFs in addition to the weak binding force between graphene sheet layers. The change of some of the H-CNFs to translucency is very interesting. One possible explanation might be that the decomposition process such as fragmentation from single crystal and decrystallization to amorphous H-CNFs were involved in the change of structure and consequently imaging. We are going to study the change by experiment throughout the long term in the future.

H-CNFs in the subcutaneous tissue did not induce an acute severe inflammatory reaction. They were englobed by phagocytes such as macrophages and foreign body giant cells.

Acknowledgment. This work was supported by Health and Labor Sciences Research Grants in Research on Advanced Medical Technology in Nanomedicine Area from the Ministry of Health, Labor and Welfare of Japan.

References

(1) Mattson, M.; Haddon, R. C.; Rao, A. M. *J. Mol. Neurosci.* **2000**, *14*, 175.
(2) Elias, K. L.; Price, R. L.; Webster, T. J. *Biomaterials* **2002**, *23*, 3279.
(3) Price, R. L.; Waid, M. C.; Haberstroh, K. M.; Webster, T. J. *Biomaterials* **2003**, *24*, 1877.
(4) Nakamura, E.; Isobe, H. *Acc. Chem. Res.* **2003**, *36*, 807.
(5) McKenzie, J. L.; Waid, M. C.; Shi, R.; Webster, T. J. *Biomaterials* **2004**, *25*, 1309.
(6) Hu, H.; Ni, Y.; Montana, V.; Haddon, R. C.; Parpura, V. *Nano Lett.* **2004**, *4*, 507.
(7) Uo, M.; Akasaka, T.; Rosca, I.; Watari, F.; Yokoyama, A.; Omori, M.; Sato, Y.; Tohji, K. Abstract No 467; *205th Meeting of The Electrochemical Society*, meeting abstracts, MA 2004-01.
(8) Sato, Y.; Ohtsubo, M.; Shinoda, K.; Jeyadevan, B.; Tohji, K.; Motomiya, K.; Yamamoto, G.; Hashida, T.; Omori, M.; Yokoyama, A. Abstract No 584; *205th Meeting of The Electrochemical Society*, meeting abstracts, MA 2004-01.
(9) Yamago, S.; Tokuyama, H.; Nakamura, E.; Kikuchi, K.; Kananishi, S.; Sueki, K.; Nakahara, H.; Enomoto, S.; Ambe, F. *Chem. Biol.* **1995**, *2*, 385.
(10) Service, R. F. *Science* **1998**, *281*, 941.
(11) Huczko, A.; Lange, H.; Calko, E.; Grubek-Jaworska, H.; Droszcz, P. *Fullerene Sci. Technol.* **2001**, *9*, 251.
(12) Huczko, A.; Lange, H. *Fullerene Sci. Technol.* **2001**, *9*, 247.
(13) Tamura, K.; Takashi, N.; Kumazawa, R.; Watari, F.; Totsuka, Y. *Mater. Trans.* **2002**, *43*, 3052.
(14) Kumazawa, R.; Watari, F.; Takashi, N.; Tanimura, Y.; Uo, M.; Totsuka, Y. *Biomaterials* **2002**, *23*, 3757.
(15) Service, R. F. *Science* **2003**, *300*, 243.
(16) Schvedova, A. A.; Castranova, V.; Kisin, E. R.; Schwegler-Berry, D.; Murray, A. R.; Gandelsman, V. Z.; Maynard, A.; Baron, P. J. *Toxicol. Environ. Health A* **2003**, *66*, 1909.
(17) Covin, V. L. *Nature Biotechnol.* **2003**, *21*, 1166.
(18) Maynard, A. D.; Baron, P. A.; Foley, M.; Schvedova, A. A.; Kisin, E. R.; Castranova, V. J. *Toxicol. Environ. Health A* **2004**, *67*, 87.
(19) Warheit, D. B.; Laurence, B. R.; Reed, K. L.; Roach, D. H.; Reynolds, G. A. M.; Webb, T. R. *Toxicol. Sci.* **2004**, *77*, 117.
(20) Lam, C. W.; James, J. T.; McCuskey, R.; Hunter, R. L. *Toxicol. Sci.* **2004**, *77*, 126.
(21) Watari, F. *Abstract of Annual Meeting 2002 of Health and Labor Sciences Research Grants in Research on Advanced Medical Technology in Nanomedicine Area from the Ministry of Health, Labor and Welfare of Japan*, 2003.
(22) Fugetsu, B.; Satoh, S.; Iles, A.; Tanaka, K.; Nishi, N.; Watari, F. *Analyst* **2004**, *129*, 565.
(23) Sato, Y.; Jeyadevan, B.; Tohji, K.; Tamura, K.; Akasaka, T.; Uo, M.; Yokoyama, A.; Shibata, K.; Watari, F. *Abstract No. 4186; 206th Meeting of The Electrochemical Society*, meeting abstracts, MA 2004-02.
(24) Rodriguez, N. M. *J. Mater. Res.* **1993**, *8*, 3233.
(25) Rodriguez, N. M.; Chambers, A.; Baker, R. T. *Langmuir* **1995**, *11*, 3862.
(26) Jonas, L.; Fulda, G.; Radeck, C.; Henkel, K. O.; Holzhunter, G.; Mathieu, H. *J. Ultra Pathol.* **2001**, *25*, 375.
(27) Wang, J. C.; Yu, W. D.; Sandhu, H. S.; Betts, F.; Bhura, S.; Delamarter, R. B. *Spine* **2000**, *24*, 899.
(28) Liu, Z.; Ooi, K.; Kanoh, H.; Tang, W.; Tomida, T. *Langmuir* **2000**, *16*, 4154.
(29) Toomey, R.; Freidank, D.; Ruhe, J. *Macromolecules* **2004**, *37*, 882.
(30) Valberg, P. A.; Albertini, D. F. *J. Cell Biol.* **1985**, *101*, 130.

NL0484752

Available online at www.sciencedirect.com
SCIENCE DIRECT
Journal of Colloid and Interface Science 275 (2004) 113–122
JOURNAL OF Colloid and Interface Science
www.elsevier.com/locate/jcis

Extension of Colacicco's experiment supporting the adsorption theory

Hirohisa Tamagawa * and Fumio Nogata

Department of Human and Information Systems, Faculty of Engineering, Gifu University, 1-1 Yanagido, Gifu 501-1193, Japan

Received 23 September 2003; accepted 20 January 2004
Available online 6 March 2004

Abstract

The pervasive concept of the cause of the potential occurring across a semipermeable membrane intervening between two ionic solutions is called the membrane theory; hence, this potential is called the membrane potential. Although almost nobody has doubted its validity, research results defying it have been continuously reported by a small number of researchers. They have claimed that the cause the potential lies in the adsorption of ions onto adsorption sites, which is the adsorption theory. One such research report by G. Colacicco (Nature 207 (1965) 936) was employed for our experimental work reported in this paper in order to examine the validity of the membrane theory and the adsorption theory. The results we obtained are in conflict with the membrane theory but appear to be in full agreement with the long dismissed adsorption theory. This paper urges the reexamination of the membrane theory and the reconsideration of the adsorption theory from a nonbiased standpoint.

Keywords: Membrane theory; Nernst equation; Hodgkin Katz Goldman equation; Adsorption theory

1. Introduction

The membrane theory has for a long while been accepted as a fully established concept for the prediction of potential behavior generated between two ionic solutions separated by a semipermeable membrane [1–8]. Indeed, its successful use is often visible. A large number of papers, textbooks, technical books, small explanatory articles, etc. have been readily at hand. Although the membrane theory is seemingly categorized in electrochemistry or physical chemistry [9], namely, it seems to have meaning only for pure science in the laboratory, it has profound meaning for our life. The membrane theory accounts for a large part of physiology [2,4–8], called electrophysiology. The function of the nervous system in the human body has been analyzed primarily based on the membrane theory, and it is reduced to actual benefits for our own life. So the membrane theory has a strong connection to us. Therefore, deepening the understanding of the membrane theory even more must be quite profitable. However, some people have denied the membrane theory [1–5,7,8,10–12], and they have advocated an alternative theory, the adsorption theory. They say that the potential generation across the semipermeable membrane is caused not by the selective permeability of the membrane, as the membrane theory predicts, but by ion adsorption onto the adsorption site existing on the membrane surface. According to their claim, there are countless counterexamples to the membrane theory that are in full agreement with the adsorption theory. However, they have all been dismissed for decades, while a great number of evidences in line with the membrane theory alone have attracted strong attention [2,4,5,7,8]. Although the adsorption theory has been out of researchers' attention nowadays, a reconsideration of it provokes the thought to us that the adsorption theory even has aspects superior to the membrane theory in explain potential behavior across semipermeable membranes.

In this work, we modified experimental work performed by Colacicco [1], which denies the membrane theory and validates the adsorption theory, into a more generalized one and examined the validity of the membrane theory again. We suggest the necessity of reconsideration of the adsorption theory.

2. Methods and materials

Basically we followed the Colacicco procedure [1]. Two compartments containing ionic solutions are contacted with

* Corresponding author.
E-mail address: tmgwhrhs@cc.gifu-u.ac.jp (H. Tamagawa).

0021-9797/$ – see front matter
doi:10.1016/j.jcis.2004.01.038

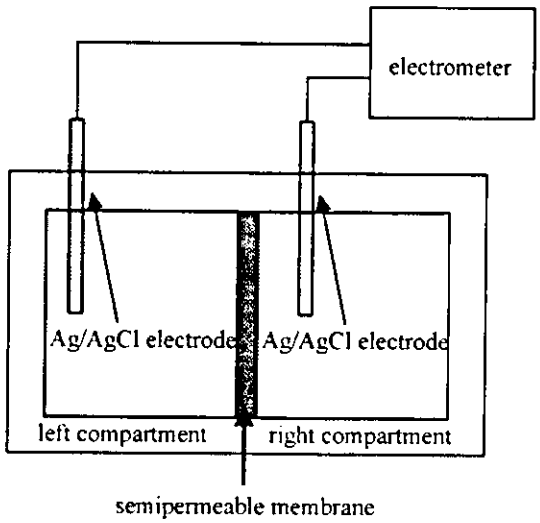

Fig. 1. The apparatus employed for the measurement of the potential generated by two ionic solutions separated by a semipermeable membrane.

each other through the intermediary of a semipermeable membrane. We employed a number of different species and concentrations of ionic solutions to fill the compartments, and we also employed several different membranes as semipermeable membranes separating two ionic solutions in the compartments. We measured the potential across the membrane by inserting Ag/AgCl electrodes into each compartment and examined the potential behavior, where all the potential measurements were performed at room temperature.

3. Results and discussion

3.1. Potential across neutral, anionic, and cationic membranes

Employing the apparatus depicted in Fig. 1, the potential generated by two ionic solutions separated by a semipermeable polymer membrane was measured, where the potential, V_{exp}, was defined by V_{exp} = (potential of the right compartment) − (potential of the left compartment) for the whole potential measurements described in this paper unless additional comments are given. We employed three different types of semipermeable polymer membranes, dialysis membrane, Nafion (DuPont, DE, USA), and Selemion (Asahi Glass Co., Tokyo, Japan). Dialysis membrane is a neutral membrane, and Nafion is a negatively charged membrane. For Selemion, we used a positively charged membrane, although both negatively and positively charged Selemion are commercially available.

Tables 1–3 show the measured potential along with the type and the concentration of ionic solutions supplied in the left and right compartments of the experimental apparatus. These potential behaviors are normally explained by the membrane theory—the Nernst equation or its generalized expression, the Hodgkin–Katz–Goldman equation

Table 1
The potential across dialysis membrane

Notation	Left solution	Right solution	V_{exp} [mV]	V_{cal} [mV]
d1	0.01 M KCl	0.10 M KCl	−4	0
d2	0.05 M KCl	0.10 M KCl	−4	0
d3	0.10 M KCl	0.10 M KCl	−3	0

Notes. Left solution ≡ the type of solution and its concentration in the left compartment. Right solution ≡ the type of solution and its concentration in the right compartment. V_{exp} ≡ the experimentally measured potential across the dialysis membrane. V_{cal} ≡ the theoretically calculated potential across dialysis membrane based on the membrane theory, assuming the dialysis membrane is quite permeable to K^+ and Cl^-.

(HKG equation) [2,4,8]. First, we try to explain these potential behaviors employing the HKG equation of the membrane theory as below.

3.1.1. Potential across the dialysis membrane

The potentials of d1, d2, and d3 in Table 1 are explained employing the HKG equation:

$$V = (RT/F)\ln\left[\left(\sum_i P_{a_i^+}[a_i^+]_l + \sum_j P_{a_j^-}[a_j^-]_r\right) \Big/ \left(\sum_m P_{a_m^-}[a_m^+]_r + \sum_n P_{a_n^-}[a_n^-]_l\right)\right]. \quad (1)$$

R, T, and F are the gas constant, the absolute temperature, and the Faraday constant, respectively. $[a_\alpha^+]_\beta$ and $[a_\alpha^-]_\beta$ are the activity of the cation of a_α^+ and of the anion of a_α^-, respectively, where β (= l and r) denotes the left compartment and the right compartment, respectively. $P_{a_\alpha^+}$ and $P_{a_\alpha^-}$ are the permeability constants of a_α^+ and a_α^- through the membrane, respectively.

This equation is, for instance, applied to d1, giving the theoretically calculated potential, V_{cal}, where V_{cal} of d1 is expressed by $V_{cal}(d1)$, and hereafter the way of this expression is employed for the representation of the potential:

$$V_{cal}(d1) = (RT/F)\ln\left[\left(P_{K^+}[K^+]_l + P_{Cl^-}[Cl^-]_r\right) \Big/ \left(P_{K^+}[K^+]_r + P_{Cl^-}[Cl^-]_l\right)\right]. \quad (2)$$

If K^+ and Cl^- both can permeate freely through the dialysis membrane, that is, the dialysis membrane does not have selective permeability, Eq. (2) is reduced to

$$V_{cal}(d1) = (RT/F)\ln\left[\left([K^+]_l + [Cl^-]_r\right) \Big/ \left([K^+]_r + [Cl^-]_l\right)\right]. \quad (3)$$

Actually, we observed no osmotic pressure across the dialysis membrane. Therefore Eq. (3) is validated. From Eq. (3), $V_{cal}(d1) = 0$ mV, which is close to the experimentally measured potential of d1, $V_{exp}(d1)$, given in Table 1. Application of the same argument to d2 and d3 results in $V_{cal}(d2) = 0$ mV and $V_{cal}(d3) = 0$ mV, where these values are shown in Table 1, too. As to the potential across the dialysis membrane, we could see good agreement between V_{exp} and V_{cal}. This suggests the validity of the membrane theory.

Table 2
The potential across Nafion

Notation	Left solution	Right solution	V_{exp} [mV]	V_{cal} [mV]
n1	0.10 M KCl	0.10 M KCl	0	0
n2	0.10 M NaCl	0.10 M NaCl	0	0
n3	0.10 M KCl	0.05 M KCl	+17	+18
n4	0.10 M KBr	0.10 M KI	+1	0
n5	0.10 M NaBr	0.10 M NaI	+2	0
n6	0.10 M KI	0.10 M NaI	+9	–
n7	0.10 M KBr	0.10 M NaBr	+9	-
n8	0.10 M NaCl: 0.10 M NaI = 1:1 in vol	0.10 M NaCl	0	0
n9	0.10 M KCl:0.10 M KI = 1:1 in vol	0.10 M KCl	+1	0
n10	0.10 M KCl	0.05 M $CaCl_2$	+10	-
n11	0.05 M $CaCl_2$	0.05 M $FeCl_2$	+18	--

Notes. Left solution ≡ the type of solution and its concentration in the left compartment. Right solution ≡ the type of solution and its concentration in the right compartment. V_{exp} ≡ the experimentally measured potential across Nafion. V_{cal} ≡ the theoretically calculated potential across Nafion based on the membrane theory assuming it is quite permeable to cations and quite impermeable to anions. The left solutions of n8 and n9 are a mixture of 0.10 M NaCl and 0.10 M NaI at a 1:1 volume ratio and a mixture of 0.10 M KCl and 0.10 M KI at a 1:1 volume ratio, respectively.

3.1.2. *Potential across Nafion*

Employing the HKG equation, we can calculate the potentials of n1–n11 as in Table 2. The potentials of n1 and n2 are theoretically calculated. We do not need to know the values of the permeability constants, since the same species and concentrations of ions are in both left and right compartments. The results are given as V_{cal} in Table 2. V_{cal} of n1 and n2 are the same as V_{exp} of them.

The experimentally obtained potentials of n3, n4, and n5 can be obtained through HKG equation, too, under a certain assumption. Nafion contains a fixed anionic group; namely, it is a negatively charged membrane. Therefore the negatively charged particles, anions, are speculated to hardly permeate through Nafion compared with the positively charged particles, cations. This speculation is interpreted as $P_{K^+} \gg P_{Cl^-}$ in case HKG equation is applied to n3. Hence, Eq. (1) is transformed into

$$V_{cal}(n3) = (RT/F)\ln\left[\left(P_{K^+}[K^+]_l + P_{I^-}[Cl^-]_r\right) \Big/ \left(P_{K^+}[K^+]_r + P_{Cl^-}[Cl^-]_l\right)\right] \approx (RT/F)\ln\left[[K^+]_l/[K^+]_r\right]. \quad (4)$$

Since the potential measurement was performed within a few minutes after the completion of setting up the experimental apparatus depicted in Fig. 1, $[K^+]_l$ and $[K^+]_r$ did not seem to change greatly from their initial concentrations. Therefore $[K^+]_l \approx 0.10$ M and $[K^+]_r \approx 0.05$ M. This gives $V_{cal}(n3) = +18$ mV, which is quite close to $V_{exp}(n3) = +17$ mV.

Applying the same argument to n4 and n5 results in the same type of equation as Eq. (4), and V_{cal} of n4 and n5 is 0 mV for both. This is quite close to V_{exp} of n4 and n5.

The same arguments applied to n3, n4, and n5 are applied to n6, too, resulting in

$$V_{cal}(n6) = (RT/F)\ln\left[\left(P_{K^+}[K^+]_l + P_{Na^+}[Na^+]_l + P_{I^-}[I^-]_r\right) \Big/ \left(P_{K^+}[K^+]_r + P_{Na^+}[Na^+]_r + P_{I^-}[I^-]_l\right)\right]. \quad (5)$$

We can immediately derive the relationship of $P_{K^+}, P_{Na^+} \gg P_{I^-}$ as to the permeability constants. Under this condition, Eq. (5) is reduced to

$$V_{cal}(n6) \approx (RT/F)\ln\left[\left(P_{K^+}[K^+]_l + P_{Na^+}[Na^+]_l\right) \Big/ \left(P_{K^+}[K^+]_r + P_{Na^+}[Na^+]_r\right)\right]. \quad (6)$$

Since we do not know the values of P_{K^+} and P_{Na^+}, we cannot proceed with their further calculation. We cannot obtain the theoretical value of $V_{cal}(n6)$. But we can speculate that P_{K^+} and P_{Na^+} are different from each other, which might cause the nonzero potential of $V_{exp}(n6) = +9$ mV in Table 2. The same argument is applicable to explain the nonzero potential of n7. Namely, each ionic species is speculated to have its own permeability constant, resulting in the nonzero potential, and that is what the HKG equation is based on.

The experimentally measured potentials of n8 and n9 are the same as or quite close to 0 mV; we can virtually see them as 0 mV, although the ionic species of the right compartment of n8 and n9 are different from those of the left compartment. Considering the argument so far, we can speculate that the cations play the predominant role in the determination of potential behavior. Taking up n8, the cation species and its concentration in both left and right compartments are exactly the same, Na^+ of 0.10 M. With these facts in mind, we can derive

$$V_{cal}(n8) \approx (RT/F)\ln\left[[Na^+]_l/[Na^+]_r\right]. \quad (7)$$

Since the potential measurement was performed within a few minutes after the completion of setting up the experimental apparatus depicted in Fig. 1, $[Na^+]_l$ and $[Na^+]_r$ did not seem to change greatly from their initial concentrations. Thus $V_{cal}(n8) \approx 0$ mV, which agrees with $V_{exp}(n8) = 0$ mV. The same argument is applicable to n9, too.

V_{cal} of n10 and n11 cannot be obtained theoretically for the same reason as the potential of n6 and n7. But their nonzero potentials are strongly speculated to be due to the difference of the values among P_{K^+}, $P_{Ca^{2+}}$, and $P_{Fe^{2+}}$.

3.1.3. *Potential across Selemion*

For the explanation of potentials of s1–s11, basically the same argument to n1–n11 are applicable.

Employing the HKG equation, we can calculate the potential of s1 and s2 theoretically as 0 mV for both, which is shown as V_{cal} in Table 3. We do not need to know the values of the permeability constants of ions for this calculation owing to the same argument given for the calculation of $V_{cal}(n1)$ and $V_{cal}(n2)$.

Table 3
The potential across Selemion

Notation	Left solution	Right solution	V_{exp} [mV]	V_{cal} [mV]
s1	0.10 M KCl	0.10 M KCl	0	0
s2	0.10 M NaCl	0.10 M NaCl	0	0
s3	0.10 M KCl	0.05 M KCl	−15	−18
s4	0.10 M KBr	0.10 M KI	+15	–
s5	0.10 M NaBr	0.10 M NaI	+12	–
s6	0.10 M KI	0.10 M NaI	0	0
s7	0.10 M KBr	0.10 M NaBr	0	0
s8	0.10 M KCl	0.05 M $CaCl_2$	−2	0
s9	0.05 M $CaCl_2$	0.05 M $FeCl_2$	−2	0
s10	0.033 M $FeCl_3$	0.05 M $FeCl_2$	+2	0
s11	0.10 M KCl:0.10 KI = 1:1 in vol	0.10 M KCl	+10	–

Notes. Left solution ≡ the type of solution and its concentration in the left compartment. Right solution ≡ the type of solution and its concentration in the right compartment. V_{exp} ≡ the experimentally measured potential across Selemion. V_{cal} ≡ the theoretically calculated potential across Selemion based on the membrane theory assuming it is quite permeable to cations and quite impermeable to anions. The left solution of s11 is a mixture of 0.10 M KCl and 0.10 M KI at a 1:1 volume ratio.

The experimentally obtained potentials of s3, s6, and s7 can be obtained through the HKG equation, too, under a certain assumption. Selemion contains a fixed cationic group; namely, it is a positively charged membrane. Therefore the positively charged particles, cations, are speculated hardly to permeate through Selemion compared with the negatively charged particles, anions. This speculation is interpreted as $P_{K^+} \ll P_{Cl^-}$ in case the HKG equation is applied to s3. Hence, Eq. (1) is transformed into

$$V_{cal}(s3) = (RT/F)\ln\left[\left(P_{K^+}[K^+]_l + P_{I^-}[Cl^-]_r\right) \Big/ \left(P_{K^+}[K^+]_r + P_{Cl^-}[Cl^-]_l\right)\right] \approx (RT/F)\ln\left[[Cl^-]_r/[Cl^-]_l\right]. \quad (8)$$

Since the potential measurement was performed within a few minutes after the completion of setting up the experimental apparatus depicted in Fig. 1, and $[Cl^-]_r$ and $[Cl^-]_l$ did not seem to change greatly from their initial concentrations. Therefore $[Cl^-]_l \approx 0.10$ M and $[Cl^-]_r \approx 0.05$ M. This gives $V_{cal}(s3) = -18$ mV, which is quite close to $V_{exp}(s3) = -15$ mV.

Applying the same argument to s6 and s7 results in expressions similar to Eq. (8), which are only different in that Cl^- is replaced by I^- for $V_{cal}(s6)$ and Br^- for $V_{cal}(s7)$. V_{cal} of s6 and s7 is 0 mV for both, the same as V_{exp} of s6 and s7.

The same argument applied to s3, s6, and s7 is applied to s4, resulting in

$$V_{cal}(s4) = (RT/F)\ln\left[\left(P_{K^+}[K^+]_l + P_{Br^-}[Br^-]_r + P_{I^-}[I^-]_r\right) \Big/ \left(P_{K^+}[K^+]_r + P_{Br^-}[Br^-]_l + P_{I^-}[I^-]_l\right)\right]. \quad (9)$$

We can immediately speculate on the relationship of $P_{K^+} \ll P_{Br^-}, P_{I^-}$ as to the permeability constants. Under this condition, Eq. (9) is reduced to

$$V_{cal}(s4) = (RT/F)\ln\left[\left(P_{Br^-}[Br^-]_r + P_{I^-}[I^-]_r\right) \Big/ \left(P_{Br^-}[Br^-]_l + P_{I^-}[I^-]_l\right)\right]. \quad (10)$$

Since we do not know the values of P_{Br^-} and P_{I^-}, we cannot proceed with further calculation. We cannot obtain the theoretical value of $V_{cal}(s4)$. But we can speculate that P_{Br^-} and P_{I^-} are different from each other, which might cause the nonzero potential of $V_{exp}(s4) = +15$ mV in Table 3. The same argument is applicable to explain the nonzero potential of s5, too.

The potentials of s8, s9, and s10 are quite close to 0 mV; we can virtually see them as 0 mV. The ionic species of the right compartment of s8 are different from those of the left compartment. However, considering the argument so far made, we can speculate that only the anions play a predominant role in the determination of potential behavior. The anion species and its concentration in both left and right compartment are exactly the same, Cl^- of 0.10 M. With these facts in mind, we can derive

$$V_{cal}(s8) \approx (RT/F)\ln\left[[Cl^-]_r/[Cl^-]_l\right]. \quad (11)$$

Since the potential measurement was performed within a few minutes after the completion of setting up the experimental apparatus depicted in Fig. 1, $[Cl^-]_r$ and $[Cl^-]_l$ did not seem to change greatly from their initial concentrations. Thus $V_{cal}(s8) \approx 0$ mV, which is in good agreement with $V_{exp}(n8) = -2$ mV. The same argument is applicable to s9 and s10, too.

The potential of s11 cannot be obtained theoretically through the HKG equation due to the same reason for the impossibility of the calculation of the potential of s4 and s5. But its nonzero potential is strongly speculated to be due to the difference of the values between P_{Cl^-} and P_{I^-}.

The dependence of the potential across the semipermeable membranes on the ionic species shown in Tables 1–3 has been quite well known [2], and we could well explain these potential behaviors employing the membrane theory. It impresses us that the membrane theory is completely validated. Next, we examine the validity of the adsorption theory based on the modified Colacicco experiment [1].

3.2. Implications of Colacicco's experiment

Before showing our experimental results, we would like to review the Colacicco experiment [1] by employing the interpretation of Ling [2,4,5,8]. The following description is quoted particularly from Ref. [5], authored by Ling.

Colacicco performed an investigation on the potential difference between two aqueous KCl solutions separated by an oil layer. He measured the potential between 1 and 100 mM KCl solutions separated by an oil layer. The membrane theory predicts a potential of 119 mV. Yet in fact, he observed 0 mV. This is in conflict with the membrane theory. One may argue that this disagreement is due to the impermeability of

the oil layer to both K^+ and Cl^-. Then Colacicco introduced into one compartment a small amount of anionic detergent, sodium dodecylsulfate, or SDS. SDS is an electrolyte and can create free cations in aqueous solution through its dissociation. The hydrocarbon tail of SDS is anchored in the oil layer due to its hydrophobicity, while its polar head is exposed to the aqueous solution phase due to its hydrophilicity. Therefore an anionic molecular layer of SDS is formed at the interface of aqueous solution and oil layers. With the introduction of SDS, Colacicco observed a nonzero, to be precise, a positive potential with respect to the other compartment. He also observed that this potential was sensitive to the concentration of K^+ in the compartment containing SDS but insensitive to that in the other compartment; furthermore it was insensitive to the concentration of Cl^- in both compartment. This finding suggests that this potential was created only at the interface of aqueous solution and oil layers with SDS, and it is more as if the potential is determined independent of the compartment without SDS.

He performed another experiment. He introduced into the compartment a small amount of cationic detergent, cetyltrimethylammonium bromide or CTAB, instead of SDS. CTAB is an electrolyte and can create a free anion in aqueous solution through its dissociation. The tail of CTAB is anchored in the oil layer due to its hydrophobicity, while its polar head is exposed to the aqueous solution phase due to its hydrophilicity. Therefore a cationic molecular layer of CTAB is formed at the interface of the aqueous solution and oil layers. With the introduction of CTAB, Colacicco observed a nonzero, to be precise, a negative potential with respect to the other compartment. He also observed that this potential was sensitive to the concentration of Cl^- in the compartment containing CTAB but insensitive to that in the other compartment; furthermore it was insensitive to the concentration of K^+ in both compartments. This finding suggests that this potential was created only at the interface of the aqueous solution and oil layers with CTAB, and the solution in the other compartment does not appear to be involved in the potential generation. So the potential is determined independent of the compartment without CTAB, as in the case of SDS introduction.

Why did the introduction of SDS (CTAB) cause the nonzero potential? Does SDS (CTAB) turn the oil layer into a membrane permeable to K^+ (Cl^-)? Such a speculation is incompatible with the experimentally observed insensitivity of the potential to the concentration of K^+ (Cl^-) in the compartment containing no SDS (no CTAB). However, without the selective permeability of the membrane to ions, the nonzero membrane potential cannot be generated according to the membrane theory.

Colacicco carried out a further experiment and found remarkable evidence defying the membrane theory. He combined the two experiments described above. He introduced SDS into one compartment and CTAB into the other compartment. If the potential generation by the introduction of either SDS or CTAB is due to the alteration of oil layer to acquire permeability to K^+ or Cl^-, respectively, the oil having both SDS and CTAB layers on its surfaces is fully permeable to both K^+ and Cl^-. So according to the membrane theory, the expected potential is 0 mV in this case regardless of the concentration of KCl in both compartments. However, Colacicco observed a quite large nonzero potential, which was close to the sum of the potentials observed in case only SDS was introduced and in case only CTAB was introduced. So Colacicco's experiment suggests that the potential long called the membrane potential is not a membrane origin potential. The potential is not determined by the selective permeability of the membrane. It is solely determined by the individual interface between the oil layer and the KCl solution. Ling suggests that the potential generation originates from the adsorption of ions onto the SDS layer and CTAB; namely, the membrane potential is, in fact, of adsorption origin, that is, an adsorption potential [2,4,5,8]. The presence of adsorption sites and ions to be adsorbed onto such adsorption sites generates the potential. Not only Ling but some other people also more or less have advocated or sided with the adsorption theory [1,3,7,10–12]. However, their efforts have been dismissed up until now. So we reconsider our observation with the adsorption theory in mind again in the subsequent sections.

3.3. Reconsideration of membrane potential

In order to enhance the implication of Colacicco's work [1] and validate the adsorption theory further, we performed the following experiments extending his work.

3.3.1. Absolute potential values

We measured the absolute potential values of several different types of ionic solutions in contact with Nafion (or Selemion). The apparatus used is the same as depicted in Fig. 1, but the left compartment is filled with the agar gel containing the saturated KCl. Through the intermediary of Nafion (or Selemion), this agar gel adjoins to the ionic solution in the right compartment. Therefore the potentials were all measured with respect to the solid agar gel phase. Table 4 shows the potentials we measured. The absolute potentials in Table 4 behave differently according to their ionic species and concentrations, and they do not seem to obey the predictions of the membrane theory. For the sake of simplicity, here we assume that there exists an invisible thin saturated 3.3 M KCl solution layer between the agar phase and Nafion (Selemion) as depicted in Fig. 2. Then we tried applying the membrane theory [2,4,6,8] to theoretically calculate the potentials in Table 4. The calculated results disagree with V_{exp}. For example, the calculated potential of n41 is +150 mV; this is totally different from $V_{exp}(n41) = +99$ mV. The calculated potential of others, V_{cal}, are also listed in Table 4 for the purpose of reference.

Table 5 shows some potential data given in Tables 2 and 3; these data are redesignated in Table 5, along with the additionally measured potentials of n512 and n513 em-

Table 4
The potential across Nafion and Selemion with respect to the agar gel containing saturated KCl

Notation	Left solution	Right solution	V_{exp} [mV]	V_{cal} [mV]
n41	saturated KCl	0.01 M KCl	+99	+150
n42	saturated KCl	0.05 M KCl	+86	+108
n43	saturated KCl	0.10 M KCl	+74	+90
n44	saturated KCl	0.01 M KI	+113	+150
n45	saturated KCl	0.05 M KI	+91	+108
n46	saturated KCl	0.10 M KI	+78	+90
n47	saturated KCl	0.01 M KBr	+104	+150
n48	saturated KCl	0.05 M KBr	+87	+108
n49	saturated KCl	0.10 M KBr	+76	+90
n410	saturated KCl	0.01 M NaI	+103	-
n411	saturated KCl	0.05 M NaI	+94	-
n412	saturated KCl	0.10 M NaI	+86	-
n413	saturated KCl	0.01 M $CaCl_2$	+108	-
n414	saturated KCl	0.05 M $CaCl_2$	+105	-
n415	saturated KCl	0.10 M $CaCl_2$	+84	-
s41	saturated KCl	0.01 M KCl	−107	−150
s42	saturated KCl	0.05 M KCl	−92	−108
s43	saturated KCl	0.10 M KCl	−77	−90
s44	saturated KCl	0.01 M KI	−119	-
s45	saturated KCl	0.05 M KI	−88	-
s46	saturated KCl	0.10 M KI	−50	-
s47	saturated KCl	0.01 M KBr	−115	-
s48	saturated KCl	0.05 M KBr	−82	-
s49	saturated KCl	0.10 M KBr	−66	-
s410	saturated KCl	0.01 M NaI	−121	-
s411	saturated KCl	0.05 M NaI	−86	-
s412	saturated KCl	0.10 M NaI	−53	-
s413	saturated KCl	0.01 M $CaCl_2$	−115	−132
s414	saturated KCl	0.05 M $CaCl_2$	−104	−90
s415	saturated KCl	0.10 M $CaCl_2$	−74	−72

Notes. Left solution ≡ the saturated KCl contained in agar gel. Right solution ≡ the type of solution and its concentration in the right compartment. V_{exp} ≡ the experimentally measured potential across the membranes. V_{cal} ≡ the theoretically calculated potential across the membranes based on the membrane theory. Nafion was used as a membrane separating the agar gel and an ionic solution for the potential measurement of n41–n415. Selemion was used as a membrane separating the agar gel and an ionic solution for the potential measurement of s41–s415.

ploying exactly the same method for the measurement of the potentials shown in Table 2. We calculated the potentials in Table 5 using the potential data in Table 4. For example, V_{cal}(n53) in Table 5 was calculated as $V_{cal}(n53) = V_{exp}(n42) - V_{exp}(n43) = +12$ mV. In the same manner, the other V_{cal} was obtained and given in Table 5. In spite of the large disagreement between the experimental results in Table 4 and their theoretical predictions by the membrane theory, V_{cal} in Table 5 calculated using V_{exp} in Table 4 is in good agreement with the corresponding V_{exp} in Table 5. So we try to explain the behavior of experimentally measured potential, V_{exp}, shown in Tables 4 and 5.

Ling suggests that the ion adsorption onto the spatially fixed adsorption sites dominates the potential behavior in the ionic solution systems [2,4,8]. Taking up V_{exp}(n51), we apply Ling's concept to it. Ionic solutions in the left and right compartments directly contact the negatively charged membrane Nafion. So Nafion offers a large number of negatively

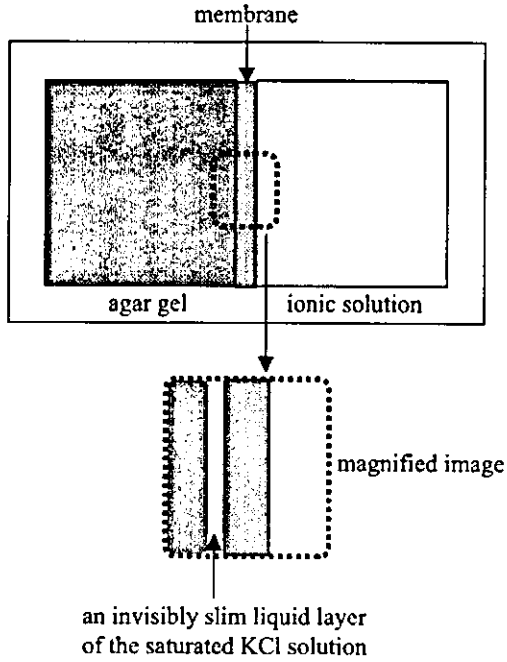

Fig. 2. The magnified image of an invisibly thin phase of saturated KCl solution speculated to be probable to occur.

Table 5
The potential across Nafion and Selemion

Notation	Left solution	Right solution	V_{exp} [mV]	V_{cal} [mV]
n51	0.01 M KCl	0.01 M KCl	0	0
n53	0.10 M KCl	0.05 M KCl	+17	+12
n54	0.10 M KBr	0.10 M KI	+1	+2
n56	0.10 M KI	0.10 M NaI	+9	+8
n510	0.10 M KCl	0.05 M $CaCl_2$	+10	+10
n512	0.10 M KCl	0.10 M KI	+2	+4
n513	0.10 M KCl	0.10 M NaI	+10	+12
s51	0.01 M KCl	0.01 M KCl	0	0
s53	0.10 M KCl	0.05 M KCl	−15	−15
s54	0.10 M KBr	0.10 M KI	+15	+16
s56	0.10 M KI	0.10 M NaI	0	−3
s58	0.10 M KCl	0.05 M $CaCl_2$	−2	+3

Notes. Left solution ≡ the type of solution and its concentration in the left compartment. Right solution ≡ the type of solution and its concentration in the right compartment. V_{exp} ≡ the experimentally measured potential across the membranes. V_{cal} ≡ theoretically calculated potential using V_{exp} in Table 4. Nafion was used as a membrane separating the agar gel and an ionic solution for the potential measurement of n51–n513. Selemion was used as a membrane separating the agar gel and an ionic solution for the potential measurement of s51–s58.

charged adsorption sites to the free cations, where they cannot be adsorption sites to the anions due to electrostatic repulsion. Therefore the potential is generated at the interfaces between the surfaces of Nafion exposed to ionic solutions in the left and right compartments. The degree of adsorption of cations onto the Nafion surfaces should depend on the concentration of cations from the view of the chemical reaction. Thus the generated potential across Nafion, V_{exp}(n51), is determined by two independent potentials, where one is

Table 6
The potential across the membrane consisting of a dialysis membrane, an agar gel containing saturated KCl, and a Nafion or Selemion

Notation	Left solution	Right solution	V_{exp} [mV]	V^l_{exp} [mV]	V^r_{exp} [mV]
n61	0.01 M KCl	0.10 M KCl	+84	0	+84
n62	0.05 M KCl	0.10 M KCl	+84	+1	+84
n63	0.10 M KCl	0.10 M KCl	+84	+1	+83
n64	0.10 M KCl	0.01 M KCl	+126	+1	+125
n65	0.10 M KCl	0.05 M KCl	+97	+1	+96
n66	0.10 M KCl	0.10 M KCl	+84	0	+84
s61	0.01 M KCl	0.10 M KCl	−76	0	−76
s62	0.05 M KCl	0.10 M KCl	−76	0	−76
s63	0.10 M KCl	0.10 M KCl	−75	0	−75
s64	0.10 M KCl	0.01 M KCl	−105	0	−105
s65	0.10 M KCl	0.05 M KCl	−87	0	−86
s66	0.10 M KCl	0.10 M KCl	−76	0	−76

Notes. Left solution ≡ the type of solution and its concentration in the left compartment. Right solution ≡ the type of solution and its concentration in the right compartment. V_{exp} ≡ the experimentally measured potential across the membrane consisting of a dialysis membrane, an agar gel containing saturated KCl, and a Nafion. V^l_{exp} ≡ the experimentally measured potential between the left compartment and the agar gel phase V^r_{exp} ≡ the experimentally measured potential between the right compartment and the agar gel phase. Nafion was used as a membrane separating the solid agar containing saturated KCl and an ionic solution for the potential measurement of n61–n66. Selemion was used as a membrane separating the solid agar containing saturated KCl and an ionic solution for the potential measurement of s61–s66. n66 is the same as n63. s66 is the same as s63.

determined at the interface between the left solution and the left surface of Nafion and the other one is determined at the interface between the right surface of Nafion and the right solution. This explanation is applicable to the other V_{exp} in Tables 4 and 5, too.

3.3.2. Influence of the ion concentration and the membrane components on the potential generation

We measured the potential generated between two adjoining KCl solutions through the intermediary of a membrane consisting of a dialysis membrane, an agar gel containing the saturated KCl, and a Nafion as depicted in Fig. 3. What is important here is that the solution in the left compartment is exposed to a quite permeable neutral dialysis membrane, while the solution in the right compartment directly contacts negatively charged membrane; that is, the solution in the left compartment can be regarded as virtually in direct contact with the agar gel. From the discussion in Section 3.3.1, the dialysis membrane has little influence on the potential. Therefore it merely plays a preventive role in the disintegration of the agar gel. The observed potentials, V_{exp}, are summarized in Table 6.

As to n61–n66 in Table 6, employing Nafion as a semipermeable polymer membrane, we can know that V_{exp} is indifferent to the KCl concentration in the left compartment from the potential behavior of n61, n62, and n63. On the other hand, we can know that it is quite sensitive to the KCl concentration in the right compartment from the potential behavior of n64, n65, and n66. Therefore the right compartment dominates the potential behavior. What is different between the right and the left compartments is the type of membrane used, that is, either dialysis membrane or Nafion. Their potentials depend solely on the right compartment where there is an interface between KCl solution and Nafion. Therefore the relationship between the ionic solution

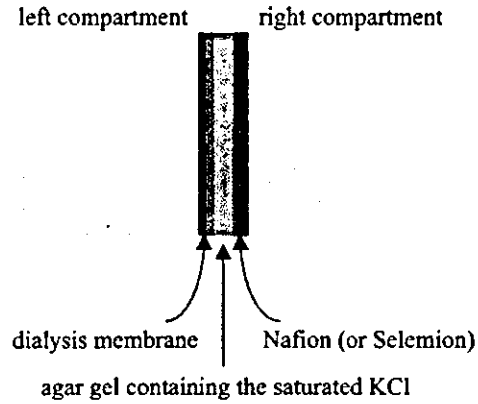

Fig. 3. The structure of membrane employed.

and the charged membrane is speculated to be responsible for the potential. This is what the adsorption theory predicts [2–5,7,8,10–12]. The same argument is applicable to the potential behavior of s61–s66 in Table 6. Their potential behavior depends solely on the right compartment, where there is an interface between the KCl solution and the positively charged membrane, Selemion. We also measured the potentials between the left compartment and the agar gel phase, V^l_{exp}, and between the agar gel phase and the right compartment, V^r_{exp}, as depicted in Fig. 4. The results are also shown in Table 6. Virtually we can interpret them as $V^l_{exp} = 0$ mV and $V_{exp} = V^r_{exp}$. Namely, the potential, V_{exp}, is undoubtedly solely determined at the interface between the right solution and Nafion (or Selemion). And we would like to add some words on this potential behavior. The individual potential of V_{exp} in Table 6 is maintained almost perfectly constant during the potential measurement. The potential deviation was within ±1 mV. This means that the KCl concentration variation in the left compartment concerning n61–n63 truly does not have even a slight influence on the behavior of V_{exp}. It is

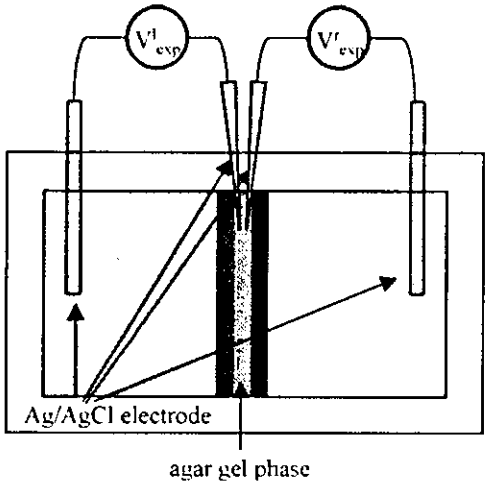

Fig. 4. The definition of V^r_{exp} and V^l_{exp}. V^r_{exp} is the potential of the right compartment with respect to the agar gel phase, and V^l_{exp} is the potential of the agar gel phase with respect to the left compartment.

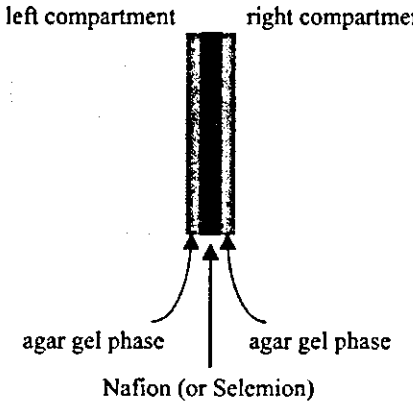

Fig. 5. The membrane of Nafion (or Selemion) sandwiched between the agar gels containing the saturated KCl solutions.

also true for s61–s63 that KCl concentration variation in the left compartment does not have any influence on the behavior of V_{exp} at all. What is important is not the selective permeability of the membrane but the existence of adsorption sites of Nafion and Selemion exposed to the ionic solution.

In order to further support the arguments above, we performed the following additional experiment. Two KCl solutions were separated by Nafion (or Selemion) fully embedded in the agar gel containing the saturated KCl as depicted in Fig. 5. We measured the potential of these KCl solutions across these membranes. The results are shown in Table 7. Two KCl solutions both in the left and the right compartments do not directly contact Nafion (or Selemion). According to the adsorption theory [1–5,7,8,10–12], the disparity of KCl concentration between two compartments cannot generate a nonzero potential because of no direct exposure of adsorption sites of Nafion (or Selemion) to KCl solution. Actually, we observed 0 mV or almost 0 mV potentials as in Table 7. It agrees with the adsorption theory, while it disagrees with the membrane theory.

Table 7
The potential across Nafion (or Selemion) embedded in the agar gel containing the saturated KCl

Notation	Left solution	Right solution	V_{exp} [mV]
n71	0.01 M KCl	0.10 M KCl	0
n72	0.05 M KCl	0.10 M KCl	0
n73	0.10 M KCl	0.10 M KCl	0
s71	0.01 M KCl	0.10 M KCl	+1
s72	0.05 M KCl	0.10 M KCl	+1
s73	0.10 M KCl	0.10 M KCl	+1

Notes. Left solution ≡ the type of solution and its concentration in the left compartment. Right solution ≡ the type of solution and its concentration in the right compartment. V_{exp} ≡ the experimentally measured potential. Employed membrane is Nafion embedded in the agar gel containing the saturated KCl for n71–n73. Employed membrane is Selemion embedded in the agar gel containing the saturated KCl for s71–s73.

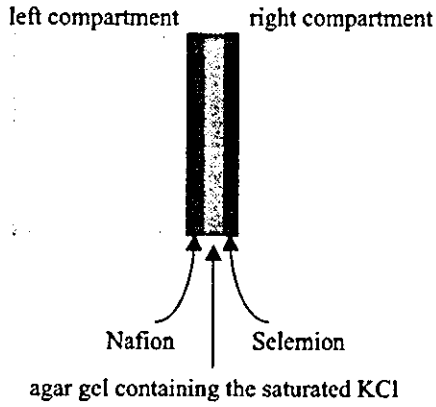

Fig. 6. The structure of the membrane employed.

3.3.3. Combination of Nafion and Selemion on the potential generation

If the adsorption theory is right rather than the membrane theory, we must be able to observe a large potential by employing the membrane with the positively charged sites on one side and the negatively charged sites on the other side as Colacicco observed [1,2,4,5,8]. We performed the following experiments to see if we can actually observe this. We measured the potential across two KCl solutions separated by the membrane consisting of a Nafion, an agar gel containing saturated KCl, and a Selemion as depicted in Fig. 6. In this case, the membrane theory predicts 0 mV as the observed potential. However, the actually observed potentials, V_{exp}, shown in Table 8, are totally different from the prediction by the membrane theory. One plausible explanation for this potential behavior could be derived from the Colacicco experiment explained in Section 3.2 [1,2,4, 5,8]. Colacicco observed the large nonzero potential generated between two KCl solutions across the oil layer with SDS and CTAB. The potential he observed was merely the sum of two potentials generated at the interfaces between KCl solution and SDS layer and between KCl solution and CTAB layer. This explanation could explain the potential behavior of V_{exp} in Table 8 in line with adsorption theory.

Table 8
The potential across the membrane consisting of Nafion, agar gel containing saturated KCl, and Selemion

Notations	Left solution	Right solution	V_{exp} [mV]	V_{cal} [mV]	V^l_{exp} [mV]	V^r_{exp} [mV]
ns1	0.10 M KCl	0.10 M KCl	−160	−151	−81	−78
ns2	0.01 M KCl	0.10 M KCl	−179	−176	−98	−78
ns3	0.10 M KCl	0.01 M KCl	−198	−181	−81	−114
ns4	0.01 M KCl	0.01 M KCl	−217	−206	−99	−116

Notes. Left solution ≡ the type of solution and its concentration in the left compartment where the left solution directly contacts Nafion. Right solution ≡ the type of solution and its concentration in the right compartment where the right solution directly contacts Selemion. V_{exp} ≡ the experimentally measured potential across the membrane consisting of Nafion, agar gel containing saturated KCl, and Selemion. V_{cal} ≡ theoretically calculated potential following Colacicco's procedure. V^l_{exp} ≡ the potential between the left compartment and the agar phase. V^r_{exp} ≡ the potential between the right compartment and the agar phase.

Following the Colacicco scheme [2], we theoretically calculated the potential, V_{cal}, for ns1–ns4. Using the potential data shown in Table 4, for instance, $V_{cal}(ns1)$ is calculated as $V_{cal}(ns1) = V_{exp}(s43) - V_{exp}(n43) = -151$ mV. All other potentials were calculated in the same manner and are summarized in Table 8. For all the cases, V_{cal} is quite close to V_{exp}. Furthermore, we measured V^l_{exp} and V^r_{exp} following the same procedure as described in Section 3.3.2. The results are given in Table 8, too. Obviously, V_{exp} is given by the sum of V^l_{exp} and V^r_{exp}. V^l_{exp} depends on KCl concentration in the left compartment and is independent of the condition of the right compartment. V^r_{exp} depends on KCl concentration in the right compartment and is independent of the condition of the left compartment. So all the potential behaviors we have observed, V_{exp}, V^l_{exp}, and V^r_{exp}, are indeed determined at the interfaces between the agar gel and Nafion and between the agar gel and Selemion, not by the selective permeability of the membrane.

3.4. Reinterpretation of the membrane potential

Extending Colacicco's work [1], we performed several experiments. Considering the results obtained up until here along with the results Colacicco obtained in his own research, the passage of ions through the membrane does not appear to affect the potential generation. Our observation suggests that one compartment containing the solution has its own potential independent of the other compartment's condition. What we measured as the membrane potential is merely the combined potentials of the two compartments, as Colacicco observed long ago. For the generation of nonzero potential, what is important must be the surface adsorption of ions on the membrane, as suggested by the proponents of the adsorption theory. In order to strongly support the meaning of ion adsorption onto the membrane the following experiment was performed.

Cheng experimentally showed that the change of ratio of the number of adsorption sites on one membrane surface to that on the opposite membrane surface, which separate two ionic solutions, can cause a potential change [11]. This strongly suggests that the adsorption sites on the membrane surfaces are involved in the nonzero potential generation, rather than the selective permeability of the membrane; that is, his research results support the adsorption theory. With

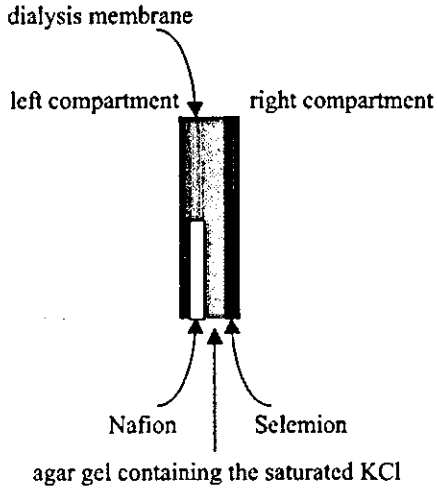

Fig. 7. The structure of the membrane employed. It has three layers. The left side consists of dialysis membrane, half of which is covered with Nafion. The middle portion is an agar gel containing the saturated KCl. The right side consists of Selemion.

Cheng's work in mind, we performed the following experiment. A membrane consisting of dialysis membrane, Nafion, Selemion, and agar gel containing saturated KCl was prepared; its structure is depicted in Fig. 7. It separates two KCl solutions. The left side of the membrane consists of a dialysis membrane half of which is covered with Nafion (see Fig. 7). This left side surface of the membrane can be regarded as quite permeable because half of it is covered with dialysis membrane only, and this area directly contacts the agar gel and KCl solution.

Table 9 is the results we obtained. dns1 and dns2 are different from each other only in the KCl concentration in the left compartment. Since the left surface of the membrane is quite permeable to ions, the semipermeable membrane is virtually Selemion only. Therefore according to the membrane theory, we can expect a potential decrease with the increase of KCl concentration in the left compartment. However, the experimentally obtained potentials of V_{exp}(dns1) and V_{exp}(dns2) have the opposite relationship. This must be caused by the role of Nafion as an adsorption site for K^+; this concept agree with the adsorption theory.

The potential of dns1 and dns2 seem to decrease slowly with time. Therefore lower potentials than V_{exp}(dns1) and

Table 9
The potential across the membrane consisting of a dialysis membrane, Nafion, the agar gel containing the saturated KCl, and Selemion

Notation	Left solution	Right solution	V_{exp} [mV]
dns1	0.01 M KCl	0.10 M KCl	−83
dns2	0.10 M KCl	0.10 M KCl	−78
dns3	0.10 M KCl	0.01 M KCl	−117
dns4	0.10 M KCl	0.10 M KCl	−78

Notes. Left solution ≡ the type of solution and its concentration in the left compartment. Right solution ≡ the type of solution and its concentration in the right compartment. V_{exp} ≡ the experimentally measured potential across the membrane consisting of a dialysis membrane, Nafion, the agar gel containing saturated KCl, and Selemion. dns4 is the same as dns2.

V_{exp}(dns2) given in Table 9 would be expected, if we waited for a long while before performing the potential measurement.

One may think that there exists a slight selective permeability for the left side membrane, and it might cause the potential change from $V_{exp}(\text{dns1}) = -83$ mV to $V_{exp}(\text{dns2}) = -78$ mV. However, the experimental observation of dns2 showed a nonzero potential, despite the same concentration of KCl in both compartments, just like the experiment ns1 in Table 8. The membrane theory cannot explain this. The relationship between V_{exp}(dns1) and V_{exp}(dns2) is also regarded as supportive evidence to the adsorption theory as explained next. V_{exp} is given by

$$V_{exp} = [\text{the potential in the right compartment}] - [\text{the potential in the left compartment}]. \quad (12)$$

Assuming the adsorption theory is valid in this experiment, [the potential in the right compartment] is speculated to be maintained constant concerning dns1 and dns2. Therefore V_{exp} of dns1 and dns2 is a function of [the potential in the left compartment] as given by

$$V_{exp} = \text{const} - [\text{the potential in the left compartment}]. \quad (13)$$

According to the potential behavior of n41 and n43 in Table 4, whose behaviors are in line with the adsorption theory as explained in Section 3.3.1, their potential decreases with increased KCl concentration from +99 to +74 mV. Employing this relationship for Eq. (13), we can obtain the relationship

$$\begin{aligned} V_{exp}(\text{dns1}) &= \text{const} - [\text{the potential of low conc. KCl in the left compartment}] \\ &< \text{const} - [\text{the potential of high conc. KCl in the left compartment}] \\ &= V_{exp}(\text{dns2}). \end{aligned} \quad (14)$$

So $V_{exp}(\text{dns1}) < V_{exp}(\text{dns2})$ is expected, and it agrees with our observation, $V_{exp}(\text{dns1}) = -83$ mV $< V_{exp}(\text{dns2}) = -78$ mV. This argument also brings us the relationship $V_{exp}(\text{dns3}) < V_{exp}(\text{dns4})$, and it agrees with the experimental results in Table 9. This evidence also strongly supports the validity of the adsorption theory.

4. Summary and conclusions

The potential of two ionic solutions across a membrane is determined by the sum of the potentials at individual interfaces between the ionic solution and the membrane, not the selective permeability of the membrane. The potential generation has nothing to do with the membrane permeability, but that there is an exposure of its adsorption sites to the ionic solution actually dominates the nonzero potential occurrence. These observations all agree with the adsorption theory but conflict with the membrane theory. We should reinterpret the results believed to be in line with the membrane theory now.

Acknowledgments

We express our gratitude to Nihon Polymer (Aichi, Japan) for their service to us many times to get Nafion sheets and also to Asahi Glass Co., Ltd. (Tokyo, Japan) for providing us Selemion sheets. This work was conducted under financial support by Health and Labor Science Research Grants of Research on Advanced Medical Technology (No. H14-nano-021) from the Ministry of Health Labor and Welfare, The Mikiya Science and Technology Foundation, and the Ogawa Foundation, all in Japan.

References

[1] G. Colacicco, Nature 207 (1965) 936.
[2] G.N. Ling, In Search of the Physical Basis of Life, Plenum, New York, 1984.
[3] K.L. Cheng, in: J.T. Stock, M.V. Orno (Eds.), ACS Symposium Series, vol. 390, 1989, p. 286.
[4] G.N. Ling, A Revolution in the Physiology of the Living Cell, Krieger, 1992.
[5] G.N. Ling, Physiol. Chem. Phys. Med. NMR 26 (1994) 121.
[6] B. Alberts, D. Bray, A. Johnson, J. Lewis, M. Raff, K. Roberts, P. Walter, Essential Cell Biology—An Introduction to the Molecular Biology of the Cell, Garland, New York, 1998 [Japanese edition, Nankodo, Tokyo, 1999].
[7] G.H. Pollack, Gels and the Engines of Life: A New, Unifying Approach to Cell Function, Ebner & Sons, Seattle, 2001.
[8] G.N. Ling, Life at the Cell and Below-Cell Level: The Hidden History of a Fundamental Revolution in Biology, Pacific Press, New York, 2001.
[9] P.W. Atkins, Physical Chemistry, second ed., Oxford Univ. Press, Northants, 1982.
[10] G. Ehrensvärd, L.G. Sillén, Nature 141 (1938) 788.
[11] K.L. Cheng, S.N. Kar Chaudhari, Microchim. Acta 1 (1981) 185.
[12] K.L. Cheng, Microchem. J. 72 (2002) 269.

Available online at www.sciencedirect.com
SCIENCE DIRECT
Journal of Colloid and Interface Science 275 (2004) 107–112
JOURNAL OF Colloid and Interface Science
www.elsevier.com/locate/jcis

An interpretation of amphoteric gel hardness variation through potential and hardness measurement

Hirohisa Tamagawa,[a,*] Fumio Nogata,[a] and Kazuyuki Yagasaki [b]

[a] *Department of Human and Information Systems, Faculty of Engineering, Gifu University, 1-1 Yanagido, Gifu 501-1193, Japan*
[b] *Department of Mechanical System Engineering, Faculty of Engineering, Gifu University, 1-1 Yanagido, Gifu 501-1193, Japan*

Received 23 September 2003; accepted 20 January 2004
Available online 5 March 2004

Abstract

The hardness variation of amphoteric gel according to the surrounding solution conditions is quite unique. It hardens and softens reversibly regardless of its molecular network density. But this has been understood merely qualitatively. For the purpose of elucidation of the details of its behavior, we performed quantitative potential and hardness measurements on it. We observed the constant potential of amphoteric gels, ~ -60 mV, regardless of their swelling ratio and hardness. Such observations can be interpreted as the maintenance of the constant charge density of $-COO^-$ for any amphoteric gel, and they are further interpreted as intermolecular salt-linkage formation/disruption dominating the hardness of amphoteric gels.

Keywords: Neutral gel; Anionic gel; Cationic gel; Amphoteric gel; Swelling ratio; Potential; Hardness; Salt linkage; Molecular network density; Cross-linking

1. Introduction

Polymer gels have quite unique properties. Their phase transition has attracted especially strong attention from a number of researchers [1,2]. Although numerous efforts have been made to elucidate amphoteric gels' nature, still it has not been well understood, and the realization of gel applications is far beyond our reach. The recent investigation of gels performed by H.T. and F.N. (two of the authors of this paper) and collaborators suggested quite intriguing facets of their hardness behavior [3,4]. We further investigated their nature and report some findings on it in this paper.

The commonly known anionic and cationic gels containing –COOH and $-NH_2$, respectively, exhibit hardness variation according to the solution conditions surrounding them [3,4]. This is explained in terms of molecular network density. Both anionic and cationic gels soften in the swollen state, that is, the low-molecular-network-density state, while they harden in the contracted state, that is, the high-molecular-network-density state. This is an intuitively acceptable explanation. Hardness of amphoteric gels containing two functional atomic groups, –COOH and $-NH_2$, varies significantly, too, according to the solution conditions surrounding them. Yet, their hardness variation cannot be explained in terms of their molecular network density, unlike that of anionic or the cationic gels. It has been suggested that amphoteric gel hardness is sometimes high even in the largely swollen state, that is, the low-molecular-network-density state. Namely, the molecular network density of amphoteric gels is not a predominant factor in their hardness. Indirect evidence was found supporting the conclusion that the cross-linking dominates the degree of amphoteric gel hardness and the amount of cross-linking reversibly varies with the environmental conditions [3,4]. As intuitively understood, the increase of gel volume results in the decrease of molecular network density, leading to the decrease of cross-linking density. But as we reported before, this phenomenon does not appear to be true for amphoteric gels, namely, the further formation of cross-linking called salt linkage appears to be promoted in amphoteric gels, even when their volume increases, consequently the cross-linking density of amphoteric gel becomes higher even in its larger volume state [3,4]. We have strongly speculated that the cross-liking density dominates the hardness of the amphoteric gel; that is, the increase of cross-linking density causes

* Corresponding author.
E-mail address: tmgwhrhs@cc.gifu-u.ac.jp (H. Tamagawa).

0021-9797/$ – see front matter
doi:10.1016/j.jcis.2004.01.039